Supplementary Material for "Direct measurement of the tunable electronic structure of bilayer MoS_2 by interlayer twist"

Po-Chun Yeh,[1] Wencan Jin,[2] Nader Zaki,[2] Jens Kunstmann[3,4],Daniel Chenet[5], Ghidewon Arefe[5], Jerzy T. Sadowski,[6] Jerry I. Dadap,[2] Peter Sutter,[7] James Hone[5], and Richard M. Osgood, Jr.[1,2,*]

[1] Department of Electrical Engineering, Columbia University, New York, New York 10027, USA

[2] Department of Applied Physics and Applied Mathematics, Columbia University, New York, New York 10027, USA

[3]Department of Chemistry, Columbia University, New York, New York 10027, USA

[4]Theoretical Chemistry, TU Dresden, 01062 Dresden, Germany

[5]Department of Mechanical Engineering, Columbia University, New York, New York 10027, USA

[6]Center for Functional Nanomaterials, Brookhaven National Laboratory, Upton, New York 11973, USA

[7]Department of Electrical and Computer Engineering, University of Nebraska-Lincoln, Lincoln, Nebraska 68588, USA

Table of contents

i. Sample Preparation

Measuring bilayer MoS_2 with different twist angles is accomplished by transferring one sheet of chemical-vapor-deposition (CVD)-grown monolayer MoS_2, on top of second sheet, which is itself mounted on a native-oxide Si substrate [1,2]. The monolayer CVD MoS_2 samples were prepared using the solid precursor growth technique[3] on a 285nm-SiO_2-coated Si chip. The growth substrates were pre-cleaned in acetone and isopropanol, followed by 2 hr rinsing in Piranha solution and 2 minutes of O_2 plasma etching. More details on the growth procedure can be found in Ref. 3. The CVD growth yields monolayer samples of MoS_2, each with differently shaped flakes ranging from triangular/polygonal islands to large continuous patches. The thickness of the sample is examined by Raman and photoluminescence spectroscopy[4,5] prior to transfer. A randomly oriented sheet of ML CVD MoS_2 is then placed on a MoS_2 flake on a native-oxide Si substrate; this allows one to create arbitrary bilayer MoS_2 flakes and patches, each exhibiting a different twist angle.

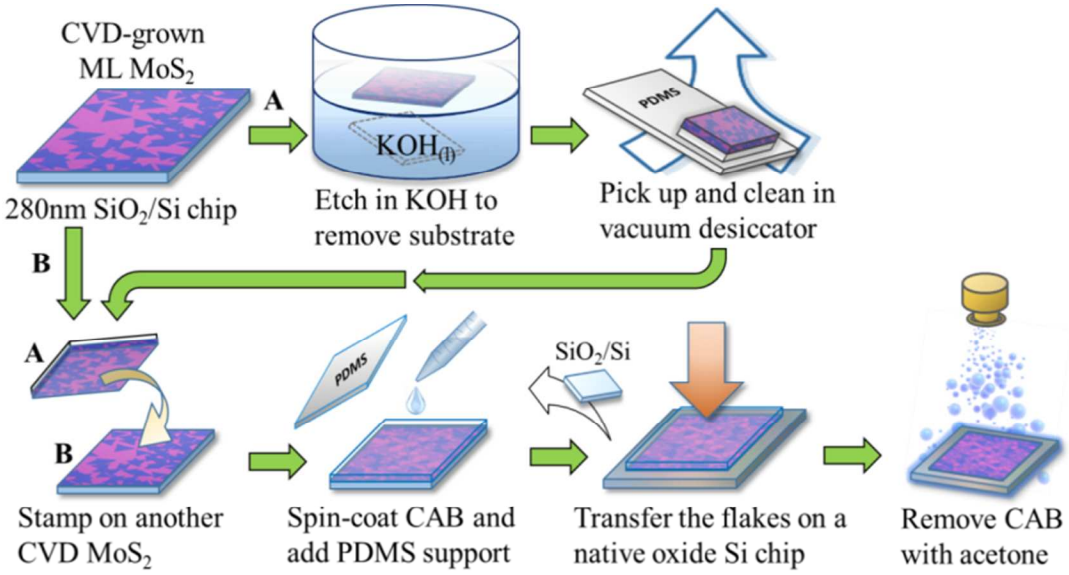

Fig. S1 The making of $TBMoS_2$ via transferring two monolayer CVD grown MoS_2 sheets on a native-oxide Si substrate. Note that the interface between the two ML MoS_2 samples remains clean during transfer since there is limited air exposure, and neither of them were exposed to any of the solutions or the etchant.

Figure S1 shows the flowchart of the transfer method. CVD grown MoS_2 on SiO_2/Si (flake A) was carefully laid afloat on a 1M KOH solution, with a PDMS stamp pressed on the MoS_2 surface to support the flakes and to protect the surface cleanness. A KOH solution etched away the SiO_2 epi-layer, causing the chips to fall off, and leaving the PDMS/MoS_2 stack in solution. Later, the stack was rinsed with DI water, left to dry for a day, and scooped up using a PDMS sample holder. After removing the first PDMS cover from the stack, the MoS_2 was cleaned in a vacuum desiccator, and then was stamped onto another CVD MoS_2 (flake B) on SiO_2/Si. Notice that the interface of the two MoS_2 monolayers are clean and untouched by any solution. Now, the PDMS sample holder used earlier was removed from the MoS_2/MoS_2/substrate stack and a layer of cellulose acetate butyrate (CAB) polymer was spin-coated on top of the stack. Extra CAB polymer was cut out, leaving only a square of CAB covering the MoS_2 flakes. The cut was exposed to water to help peel off the SiO_2/Si substrate. Note that the MoS_2 flakes preferentially attach to the CAB film instead of the SiO_2/Si substrate. The CAB/MoS_2/MoS_2 stack was then stamped on a native-oxide Si substrate that has been cleaned and pre-patterned with Au alignment marks. Finally, the entire chip was immersed in acetone to dissolve the CAB layer, then rinsed in DI water, and then dried in a vacuum desiccator to complete the transfer.

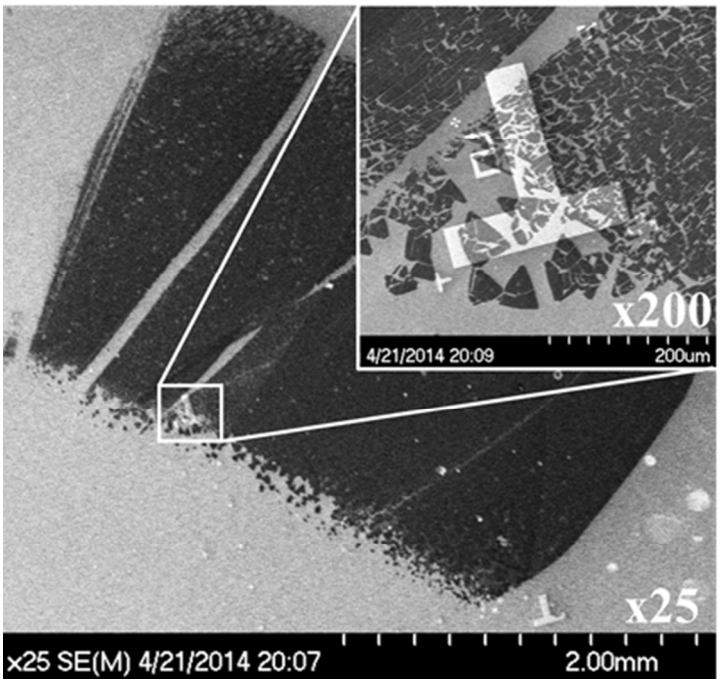

Fig. S2 SEM image of post-transferred TBMoS_2 at x25 and x200 (inlet) magnification. The CVD-grown MoS_2 exhibits triangular or polygonal shapes, which can be clearly seen. The electron energy used here is 10 keV.

ii. LEEM and ARPES Measurements

As reported earlier in LEEM, PEEM, ARPES measurements[1,6], CVD-grown MoS_2 has comparable physical and electronic properties as high quality, exfoliated MoS_2 flakes; Raman and PL spectroscopy were used extensively to check the quality and thickness of the CVD-grown samples, as mentioned above.

Our measurements were performed using the spectroscopic photoemission and low-energy electron microscope (SPE-LEEM) system at the National Synchrotron Light Source (NSLS), beamline U5UA[7]. The spectrometer energy step of the instrument was set to a 100 meV at 42 eV incident photon energy with a beam spot size of 100 μm. The momentum resolution in μ-ARPES is ~0.02 $Å^{-1}$, and the spatial resolution was determined by a selected-area aperture with an effective size of 2 μm on the sample. The TB-MoS_2 samples were stacked and pre-transferred to a native-oxide-covered Si substrate (as mentioned above). After transfer, the sample was checked by scanning electron microscopy (SEM) (Fig. S2) and LEEM (Fig. 1(a)) to confirm a successful transfer, since few-layer MoS_2 films lack optical contrast on a native-oxide Si substrate. The sample preparation and cleaning procedure are also essential to yield high-quality ARPES results. Prior to measurements, the post-transferred samples were rinsed in acetone for 24 hours, and then annealed at 350°C for ~12 hours under UHV conditions to remove contaminants. Additional experimental details regarding sample preparation can be found above and in Refs. 2,3,4,6. BF- and DF-LEEM as well as PEEM (not shown) were utilized as they provide

rich information on surface morphology, work function, etc. from the post-transferred TB-MoS_2 (Fig. 1(a)-(d)).

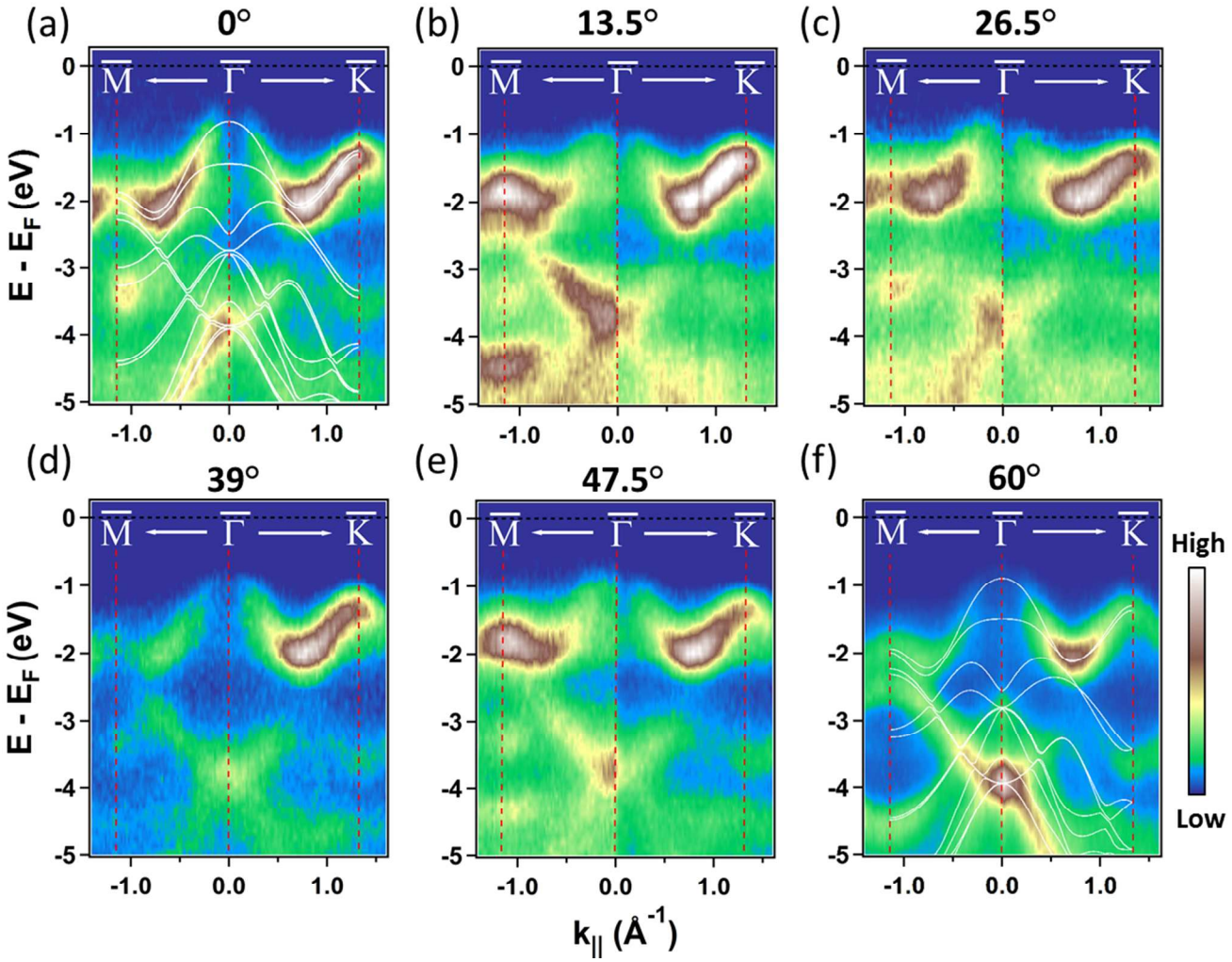

Fig. S3 μ-ARPES measurements of $TBMoS_2$ cut along $\bar{M}$-$\bar{\Gamma}$-$\bar{K}$ at (a) 0° (b) 13.5° (c) 26.5° (d) 39° (e) 47.5° (f) 60°. The overlaying white lines are DFT-calculated bands. ARPES intensity maps were normalized for each direction, $\bar{\Gamma}$-$\bar{K}$ and $\bar{\Gamma}$-$\bar{M}$, independently to achieve better contrast. Note that the bands, in this case, were referenced with respect to the Fermi level.

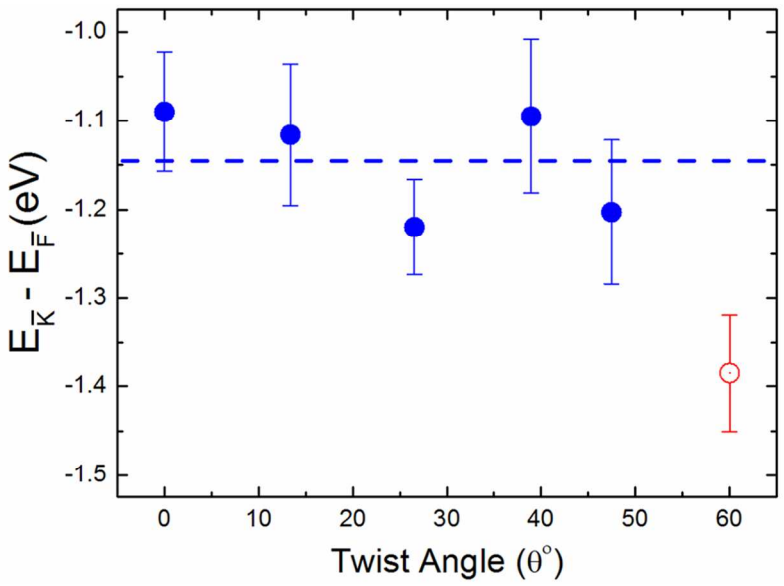

Fig. S4 Energy difference between $\bar{K}$ and Fermi level. There are no obvious correlation versus twist angle. Note that the 60 degree data point is derived from an exfoliated sample while the blue data points are derived from CVD-grown MoS_2; the relatively large difference between exfoilated and CVD data points implies that the exfoliated sample was more electron doped.

iii. Further discussion and analysis of energy differences

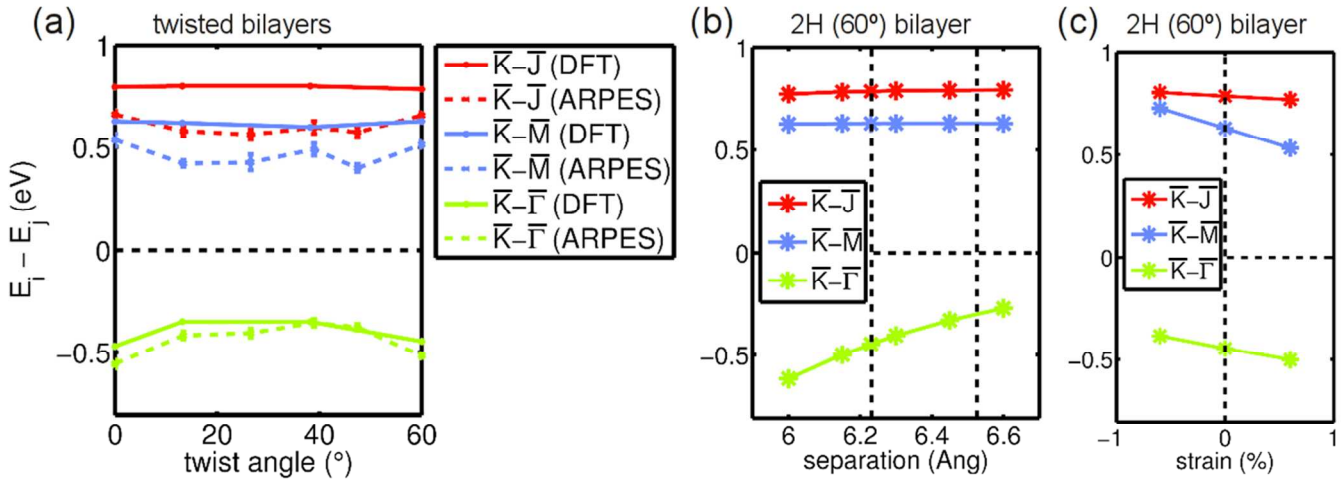

Fig. S5 Band energy differences calculated with density functional theory (DFT) employing a model of free-standing MoS_2 bilayers.

(a) Comparison of energy differences for twisted bilayers: DFT vs. ARPES. The DFT model calculations agree well with ARPES for $\bar{K}$-$\bar{\Gamma}$, however for $\bar{K}$-$\bar{J}$ and $\bar{K}$-$\bar{M}$ the model cannot fully capture the values of the energy differences as well as the variations with angle (see also Fig. 3(c) and 4(a) of the main article).
(b) The change of the energy differences with layer separation in a 60° bilayer; dashed vertical lines correspond to the equilibrium separations of twisted bilayers at 60° (6.23 Å) and 30° (6.53 Å). Only $\bar{K}$-$\bar{\Gamma}$ is sensitive to a change in the bilayer separation while the $\bar{J}$ and $\bar{M}$ point related energies are insensitive. The reason for this difference is the orbital character of the related band states as shown in Fig. 2(a) of the main article: The $\bar{\Gamma}$ point state involves inner sulfur p_z states and it is influenced by their orbital overlap, which depends on the bilayer separation. The $\bar{J}$ and $\bar{M}$ states mostly involve Mo *d* states which are well separated from their counterparts in the other layer and are therefore insensitive to changes of the layer separation. Thus the mismatch between DFT and ARPES for $\bar{K}$-$\bar{J}$ and $\bar{K}$-$\bar{M}$ is not related to the interlayer separation.
(c) The effect of homogeneous in-plane strain on the energy differences in a 60° bilayer. $\bar{K}$-$\bar{\Gamma}$ and $\bar{K}$-$\bar{M}$ are most sensitive to strain and $\bar{K}$-$\bar{J}$ is significantly less sensitive. The excellent agreement for $\bar{K}$-$\bar{\Gamma}$ in (a) is obtained from unstrained models. Application of large strains would modify both $\bar{K}$-$\bar{\Gamma}$ and $\bar{K}$-$\bar{M}$. This suggests that the mismatch for $\bar{K}$-$\bar{J}$ and $\bar{K}$-$\bar{M}$ in (a) may not be related to strain; one possibility for the mismatch may be the presence of sulfur vacancies; further investigation, which his beyond the scope of this paper, is required.

To allow for a proper comparison of the DFT band structure near $\bar{\mathrm{K}}$ with the experimental values, our DFT calculations are done without including spin-orbit coupling (SOC). In a monolayer the inclusion of SOC splits the $\bar{\mathrm{K}}$ state into two bands, with an energy separation of about 0.15 eV. In a bilayer the number of bands doubles and there are four bands near $\bar{\mathrm{K}}$ (two of them are usually degenerate, depending on the symmetry of the bilayer). The SOC splitting is below the experimental

resolution and therefore the extracted energy position of $\bar{K}$ corresponds to an average of the 4 individual band energies. As inclusion of SOC splits the bands symmetrically, the average of the 4 individual band energies is equivalent to the band energy, calculated without SOC. To check this, we did DFT band structure calculations with and without SOC for the 0°, 13.2° and 60° bilayer. The averaged band energies and the hole effective masses obtained from calculations with SOC indeed turned out to be nearly identical to the values obtained without SOC. Furthermore the effective masses obtained from the individual bands (including SOC) are quite similar and maximally vary over a range of 0.08 m_e. Thus the inclusion of SOC does not lead to strong quantitative differences in the effective masses of MoS_2 bilayers.

Note that the valence band states at $\bar{\Gamma}$ are derived from out-of-plane Mo d_{z^2} and S p_z orbitals, while those in the region in between $\bar{\Gamma}$ and $\bar{K}$, i.e., near the $\bar{J}$ state, are gradually changing from a mixture of in-plane and out-of-plane Mo $d_{x^2-y^2/xy}$, d_{z^2} orbitals, to solely in-plane Mo $d_{x^2-y^2/xy}$ orbitals at $\bar{K}$. As for the $\bar{M}$ state, it mostly consists of out-of-plane Mo d_{xy}, d_{z^2} and S p_z orbitals (see Fig. 2a).

iv. Effective mass

In the analysis of the effective mass, the in-plane bulk lattice constant of MoS_2 a = 3.16Å was used. Assuming that this in-plane lattice constant changes by ±5%, the effective mass values reported in the text would change by ~11%. Note that this value is less than our reported errors.

Twist angle (°)	$\bar{\Gamma}$	$\bar{K}$
0	1.07	0.58
13.2	1.44	0.57
21.8	1.53	0.58
27.8	1.53	0.58
32.2	1.51	0.58
38.2	1.50	0.58
46.8	1.43	0.57
60	1.08	0.58

Table S1 Hole effective masses (in units of the free electron mass m_e) at the $\bar{\Gamma}$ and at the $\bar{K}$ of twisted bilayers calculated with density functional theory (DFT) employing a model of free-standing MoS_2 bilayers. Within the DFT model the effective mass at $\bar{\Gamma}$ changes with twist angle and it is almost constant at $\bar{K}$. The corresponding values for the MoS_2 monolayer are 2.97 and 0.58 for $\bar{\Gamma}$ and $\bar{K}$, respectively.

v. Determination of energy difference between $\bar{\Gamma}$ and $\bar{K}$ using EDCs peak fitting

To determine the energy difference between $\bar{\Gamma}$ and $\bar{K}$, we use EDC peak fitting to extract the energy position of the valence band maximum. As shown in Fig. S6(a), in the vicinity of $\bar{\Gamma}$ (red dashed

rectangle), there are two bands at binding energies 1eV and 1.7eV, therefore, a double Gaussian model is applied in this region. Figure S6(b) shows the raw EDCs and double Gaussian fitting in the vicinity of $\bar{\Gamma}$. The two bands are extracted from the double Gaussian peaks and denoted as band1 and band2 in Fig. S6(c). A parabola and straight line are applied to fit band1 and band2, respectively. As a result, the energy position of the valence band maximum at $\bar{\Gamma}$ is extracted to be -0.95eV. Gaussian peak fitting also extracts the energy position of valence band maximum at $\bar{K}$ (denoted as red dashed line in Fig. S6(a)) as -1.39eV. Therefore, the energy difference between $\bar{\Gamma}$ and $\bar{K}$ is 0.44eV for the 0° twist angle case. Similarly, we extract the energy difference between $\bar{\Gamma}$ and $\bar{K}$ for the other twist angles, which are shown in Fig. S6 (e)-(i).

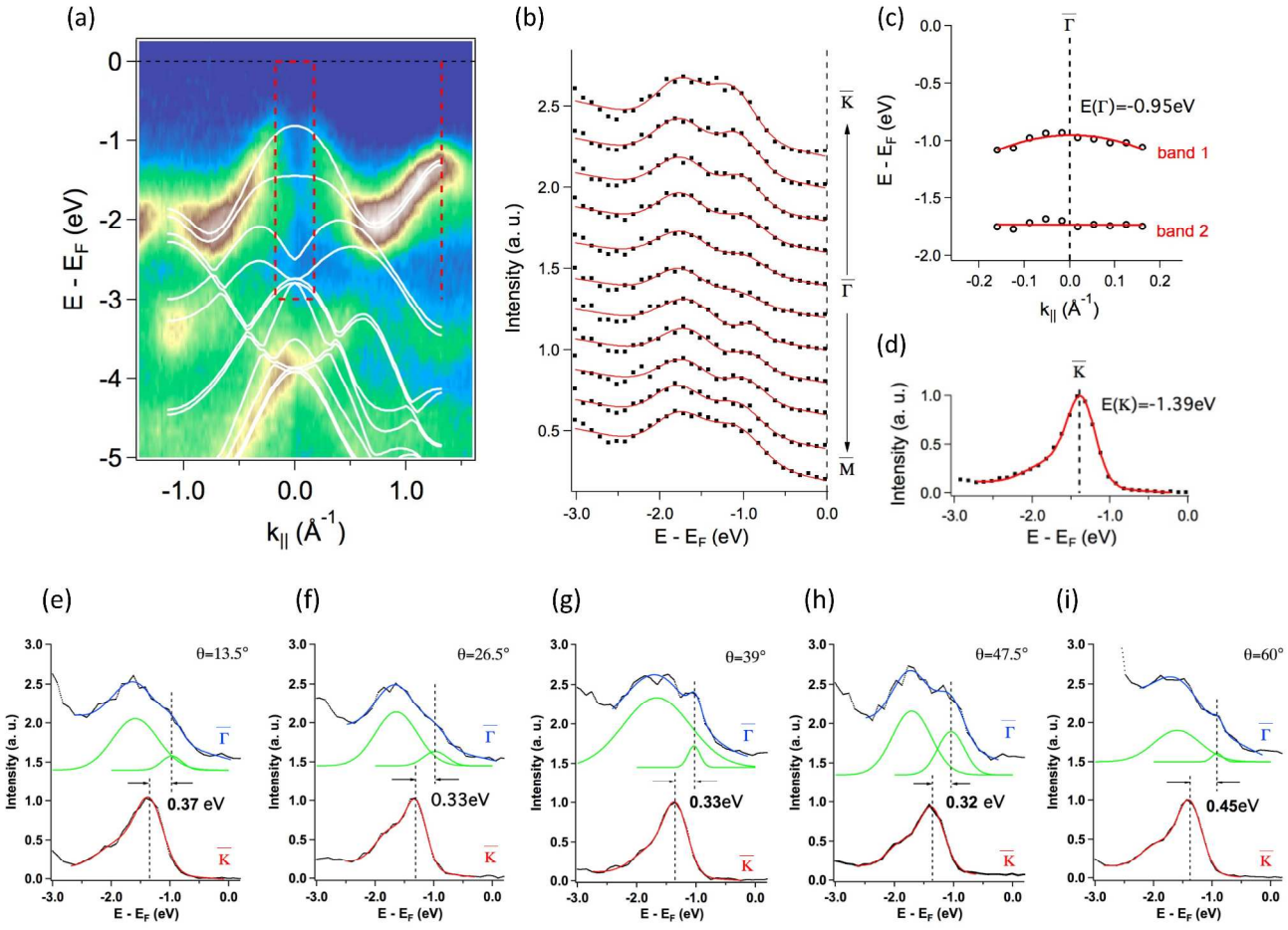

Fig. S6. (a) ARPES bandmap of TB-MoS2 with 0° twist angle. (b) Double Gaussian peak fitting of the EDCs in the range enclosed by the rectangular shown in (a). (c) Band1 and band2 extracted from the EDCs' peaks in (b). Parabola and straight line are applied to fit band1 and band2, respectively. (d) Gaussian fitting of the EDC at $\bar{K}$ (red dashed line in (a)). (e)-(i) EDC peak fitting of the 13.5°, 26.5°, 39°, 47.5°, and 60°, respectively.

vi. Details of the density functional theory calculations

Density functional theory (DFT) calculations were done with the PBE[8] generalized gradient approximation for the exchange-correlation functional and DFT-D2 dispersion corrections[9] using the PAW method[10] and a plane wave basis set with a cutoff energy of 280 eV as implemented in the VASP package[11,12]. For the k-point sampling an in-plane sampling density of 0.1/Å^2 was used. The k-space integration was carried out with a Gaussian smearing width of 0.05 eV for all calculations. All unit cells were built with 16 Å separation between replicas in the perpendicular direction to achieve negligible interaction. All systems were fully structurally optimized until all interatomic forces are below 0.01 eV/Å. Spin-orbit interactions were not taken into account because the experimental energy resolution is not resolving this effect (see discussion in section iii). For rotated bilayers commensurate supercells for special twist angles (see Fig. S1 of Ref. 10 of the main article) were constructed, following procedures developed for bilayer graphene[13]. For the relative shift of the bilayers in the lateral direction we used the configuration that has at least one point within the unit cell where a sulfur atom of one layer is placed on top of a molybdenum atom of the other layer. This configuration was found to minimize the interlayer separation.

References:

1. Jin, Wencan; Po-Chun Yeh, Nader Zaki, Datong Zhang, Jerzy T. Sadowski, Abdullah Al-Mahboob, Arend M. van Der Zande, *et al., Physical Review Letters* **2013**, 111(10), 106801.
2. van der Zande, Arend M.: Pinshane Y. Huang, Daniel A. Chenet, Timothy C. Berkelbach, YuMeng You, Gwan-Hyoung Lee, Tony F. Heinz, David R. Reichman, David A. Muller, and James C. Hone, *Nature Materials* **2013**, 12(6), 554-561.
3. Splendiani, Andrea; Liang Sun, Yuanbo Zhang, Tianshu Li, Jonghwan Kim, Chi-Yung Chim, Giulia Galli, and Feng Wang, *Nano Letters* **2010**, 10(4), 1271-1275.
4. Mak, Kin Fai; Changgu Lee, James Hone, Jie Shan, and Tony F. Heinz, *Physical Review Letters* **2010**, 105(13), 136805.
5. Feenstra, R. M.; N. Srivastava, Qin Gao, M. Widom, Bogdan Diaconescu, Taisuke Ohta, G. L. Kellogg, J. T. Robinson, and I. V. Vlassiouk, *Physical Review B* **2013**, 87(4), 041406.
6. Yeh, Po-Chun; Wencan Jin, Nader Zaki, Datong Zhang, Jerzy T. Sadowski, Abdullah Al-Mahboob, Arend M. van der Zande *et al., Physical Review B* **2014***,* 89(15), 155408.
7. Sutter, P.; M. S. Hybertsen, J. T. Sadowski, and E. Sutter, *Nano Letters* **2009**, 9(7), 2654-2660.
8. Perdew, J. P.; K. Burke, M. Ernzerhof, *Physical Review Letters* **1996**, 77, 3865–3868.
9. Grimme, S., *J. Comp. Chem.* **2006**, 27, 1787.
10. Blöchl, P. E., *Physical Review B* **1994**, 50, 17953–17979.
11. Kresse, G.; J. Furthmüller, *Physical Review B* **1996**, 54, 11169–11186.
12. Kresse, G.; J. Furthmüller, *Computational Materials Science* **1996**, 6, 15–50.
13. Shallcross, S.; S. Sharma, O. Pankratov, O., *Physical Review Letters* **2008**, 101(5), 056803.